AMERICAN SOCIETY FOR MICROBIOLOGY | Applied and Environmental Microbiology®

Engineering *Escherichia coli* Nicotinic Acid Mononucleotide Adenylyltransferase for Fully Active Amidated NAD Biosynthesis

Xueying Wang,[a,b] Yongjin J. Zhou,[a] Lei Wang,[a] Wujun Liu,[a] Yuxue Liu,[a,b] Chang Peng,[a,b] Zongbao K. Zhao[a,c]

Division of Biotechnology, Dalian Institute of Chemical Physics, CAS, Dalian, People's Republic of China[a]; University of Chinese Academy of Sciences, Beijing, People's Republic of China[b]; State Key Laboratory of Catalysis, Dalian Institute of Chemical Physics, CAS, Dalian, People's Republic of China[c]

ABSTRACT NAD and its reduced form NADH function as essential redox cofactors and have major roles in determining cellular metabolic features. NAD can be synthesized through the deamidated and amidated pathways, for which the key reaction involves adenylylation of nicotinic acid mononucleotide (NaMN) and nicotinamide mononucleotide (NMN), respectively. In *Escherichia coli*, NAD *de novo* biosynthesis depends on the protein NadD-catalyzed adenylylation of NaMN to nicotinic acid adenine dinucleotide (NaAD), followed by NAD synthase-catalyzed amidation. In this study, we engineered NadD to favor NMN for improved amidated pathway activity. We designed NadD mutant libraries, screened by a malic enzyme-coupled colorimetric assay, and identified two variants, 11B4 (Y84V/Y118D) and 16D8 (A86W/Y118N), with a high preference for NMN. Whereas in the presence of NMN both variants were capable of enabling the viability of cells of *E. coli* BW25113-derived NAD-auxotrophic strain YJE003, for which the last step of the deamidated pathway is blocked, the 16D8 expression strain could grow without exogenous NMN and accumulated a higher cellular NAD(H) level than BW25113 in the stationary phase. These mutants established fully active amidated NAD biosynthesis and offered a new opportunity to manipulate NAD metabolism for biocatalysis and metabolic engineering.

IMPORTANCE Adenylylation of nicotinic acid mononucleotide (NaMN) and adenylylation of nicotinamide mononucleotide (NMN), respectively, are the key steps in the deamidated and amidated pathways for NAD biosynthesis. In most organisms, canonical NAD biosynthesis follows the deamidated pathway. Here we engineered *Escherichia coli* NaMN adenylyltransferase to favor NMN and expressed the mutant enzyme in an NAD-auxotrophic *E. coli* strain that has the last step of the deamidated pathway blocked. The engineered strain survived in M9 medium, which indicated the implementation of a functional amidated pathway for NAD biosynthesis. These results enrich our understanding of NAD biosynthesis and are valuable for manipulation of NAD homeostasis for metabolic engineering.

KEYWORDS cofactor engineering, NAD biosynthesis, protein engineering

Received 22 March 2017 **Accepted** 25 April 2017

Accepted manuscript posted online 28 April 2017

Citation Wang X, Zhou YJ, Wang L, Liu W, Liu Y, Peng C, Zhao ZK. 2017. Engineering *Escherichia coli* nicotinic acid mononucleotide adenylyltransferase for fully active amidated NAD biosynthesis. Appl Environ Microbiol 83:e00692-17. https://doi.org/10.1128/AEM.00692-17.

Editor Harold L. Drake, University of Bayreuth

Address correspondence to Zongbao K. Zhao, zhaozb@dicp.ac.cn.

NAD and its reduced form NADH serve as common cofactors for many oxidoreductases that participate in diverse metabolic pathways. Thus, the NAD(H) level and the ratio of NAD to NADH have major roles in determining the cellular redox state and metabolic flux. Therefore, balancing cofactor availability has been widely employed to control cellular physiology and to facilitate enhanced production of different metabolites (1–3).

Escherichia coli is a commonly used microbial host for production of biobased

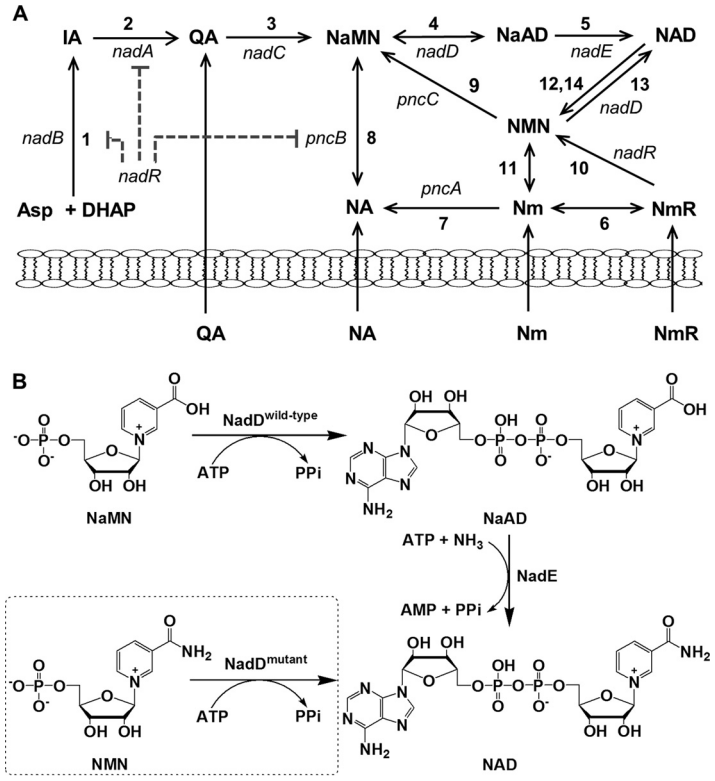

FIG 1 Pathways for NAD biosynthesis. (A) Homeostasis of NAD in *E. coli*. Asp, aspartate; DHAP, dihydroxyacetone phosphate; IA, iminoasparatate; QA, quinolinic acid; NaMN, nicotinic acid mononucleotide; NaAD, nicotinic acid adenine dinucleotide; NMN, nicotinamide mononucleotide; NA, nicotinic acid; Nm, nicotinamide; NmR, nicotinamide ribonucleoside. Enzymes: 1, L-aspartate oxidase; 2, quinolinate synthetase; 3, quinolinate phosphoribosyltransferase; 4, NaMN adenylyltansferase; 5, NAD synthetase; 6, NmR glycohydrolase; 7, Nm deamidase; 8, NA phosphoribosyltransferase; 9, NMN deamidase; 10, ribosylnicotinamide kinase; 11, NMN glycohydrolase; 12, NAD pyrophosphatase; 13, NMN adenylyltransferase; 14, DNA ligase. (B) Reactions catalyzed by NadD, NadE, and mutant NadD.

chemicals, biofuels, and pharmaceuticals due to its high growth rate, clear genetic background, and relative robustness (4, 5). In *E. coli*, NAD homeostasis is maintained via *de novo* biosynthesis, salvage pathway synthesis, and negative regulation by the repressor NadR (Fig. 1A) (6). For *de novo* NAD biosynthesis, nicotinic acid mononucleotide (NaMN) is coupled with ATP by the action of NaMN adenylyltransferase (NaMNAT; EC 2.7.7.18) to form nicotinic acid adenine dinucleotide (NaAD), which is amidated to give NAD by the action of NAD synthetase encoded by *nadE* (7). This process is known as deamidated NAD biosynthesis. Alternatively, NAD can be synthesized via the amidated pathway, where nicotinamide mononucleotide (NMN) adenylyltransferase (NMNAT; EC 2.7.7.1) is the key enzyme that directly converts NMN to NAD at the expense of ATP (8). The amidated pathway is important for NAD salvage, as it can make use of NAD degradation products, NMN, nicotinamide (Nm), and nicotinamide riboside (NmR). The *nadD* gene product NadD strongly favors NaMN over NMN and thus synthesizes NaAD 20-fold faster than NAD (9). Our previous study showed that *nadE* deletion in *E. coli* led to an NAD auxotroph phenotype and that cells failed to grow in minimal medium supplemented with NMN, indicating that native amidated pathway activity was inefficient with respect to synthesis of NAD for cell growth (10).

To expand our capacity to control cellular NAD levels, it would be interesting to have higher amidated pathway activity, which, in principle, can be achieved upon changing the NadD substrate preference for NMN (Fig. 1B). The crystal structures of *E. coli* NadD and its NaAD-NadD complex were determined previously (11). Moreover, some NadD variants have been characterized in detail (12, 13). Based on those background data, it is appealing to take a structure-guided semirational design approach (14) to generate

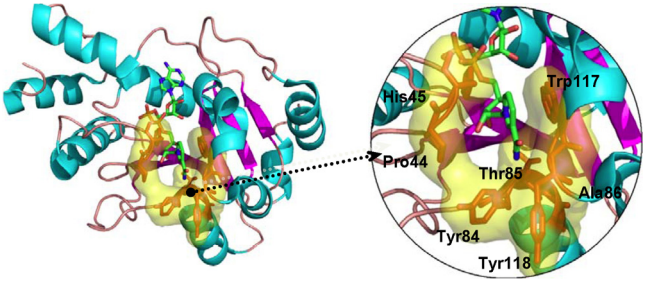

FIG 2 Crystal structure of *E. coli* NadD. The figure shows an overview of the structural architecture (left panel) and the NaMN/NMN binding domain (right panel) of NadD from *E. coli* (PDB ID: 1K4M). The residues in the binding pocket are labeled and shown as sticks (highlighted in red).

mutant libraries and to screen for NMN-preferring variants. Here, we designed NadD mutant libraries, screened by a malic enzyme-coupled colorimetric method, identified hits with high NMN preference, and established a fully active amidated NAD biosynthetic pathway. The results enriched our understanding of the molecular basis of substrate recognition by NMNAT. These mutants could be used to enhance amidated pathway activity, as an alternative to canonical *de novo* NAD biosynthesis, to manipulate the redox cofactor level for biocatalysis and metabolic engineering (15).

RESULTS

Structural analysis of NadD. The structure of the *E. coli* NadD-NaAD complex was determined previously (16). There were a number of amino acid residues involved in pyridine mononucleotide binding (Fig. 2). In particular, W117 and H45 form stacking interactions with the pyridine ring and are crucial for NaMN binding (17). In addition, T85 and Y118 create an anion pocket which forms an interaction with the exocyclic carboxylate (11). We chose to make changes at six residues (H45, P82, Y84, T85, A86, and Y118) for changing the substrate preference and devised eight double-site saturation mutant libraries, H45X/P82X, H45X/T85X, P82X/Y84X, T85X/A86X, H45X/Y118X, Y84X/Y118X, T85X/Y118X, and A86X/Y118X (where X represented any amino acid).

Mutant library construction and screening. Since undesirable residue substitution may cause frameshifts, nonsense mutations, or protein misfolding or aggregation, tracking the solubility of the mutants could reduce the workload. Inspired by studies using the green fluorescent protein (GFP) as a folding reporter (18), we fused red fluorescent protein (RFP) to the C terminus of NadD to prescreen for soluble mutants. A total of 2,000 red colonies in each library in the induced plates were selected for initial activity screening.

A colorimetric assay was performed to detect the activity by the use of coupling with a malic enzyme-catalyzed reaction and phenazine methosulfate (PMS)-mediated reduction of NBT to form formazan, a blue-colored species (Fig. 3A and B). Since crude cell lysates should contain residual NMN, initial screening assays were carried out without NMN supplementation. We obtained 297 hits in the initial screening and got 26 strains exhibiting increased activity toward NMN in the second round of verification. We then analyzed the NMN adenylyltransferase activity of crude extracts of each clone in the presence of NMN. Five mutants, namely, 8E4-RFP (Y118H), 16D8-RFP (A86W/Y118N), 4H12-RFP (A86S/Y118D), 15D1-RFP (A86S/Y118H), and 11B4-RFP (Y84V/Y118D), showed 3-fold- to 30-fold-higher activity than the wild type (Fig. 3C and Table S1). Finally, these mutants were purified to near-homogeneity (see Fig. S2A in the supplemental material), and activity was determined in the presence of 0.1 mM NMN and 2 mM ATP. Results showed that 8E4-RFP and 15D1-RFP had slightly higher activity than the wild-type NadD, while 4H12-RFP, 11B4-RFP, and 16D8-RFP showed NMN adenylyltransferase activity that was higher by 5-, 13-, and 14-fold, respectively (Fig. 3D). The activity data suggested that the Tyr-to-Asn mutation at position 118 made a major contribution to achieving better affinity for NMN.

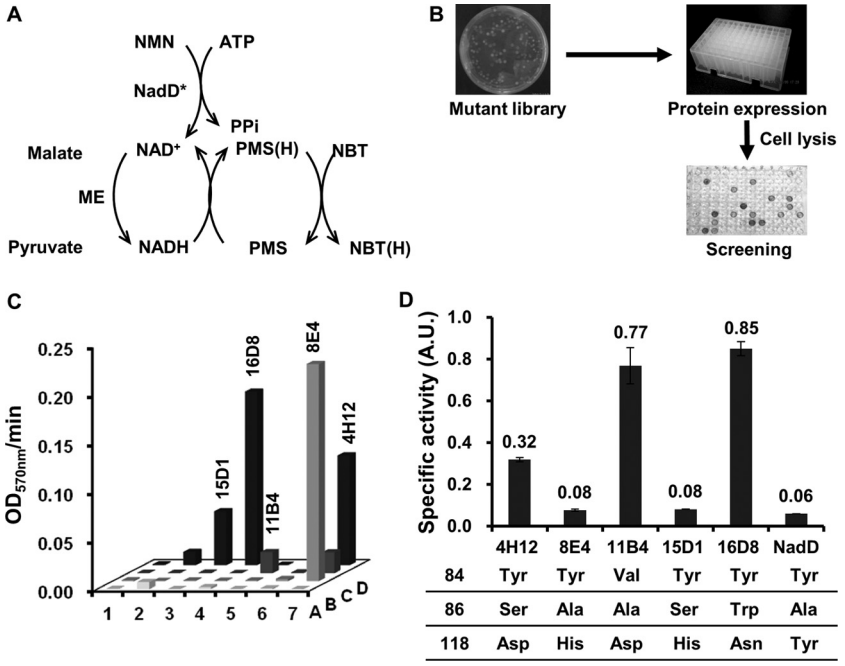

FIG 3 The process of library screening. (A) The principle of malic enzyme coupled colorimetric assay. The reaction product NAD^+ was reduced to NADH by malic enzyme, and then NBT was reduced to form insoluble blue-purple formazan in the presence of PMS. (B) Library screening process. Red colonies in the inducing plate were preselected and then cultured in the 96-well deep plate for protein expression. Cell lysates were screened by the colorimetric assay to identify hits that led to formation of blue-purple precipitates. (C) The crude enzyme activity for NMN of the mutants. The activity was measured by absorbance change in 570 nm. A1, blank; A2, DH10b harboring plasmid pUR-NadD; A3 to D7, hits that passed prescreening and cell lysate analysis. (D) Specific activity of purified enzyme for NMN. A.U., arbitrary unit.

Kinetic analysis. In order to further analyze the mutants with positive results, we expressed and purified the mutants without the RFP tag but with a His tag at the carboxy terminus (Fig. S1 and S2B). Kinetic analysis indicated that both 11B4 and 16D8 had a relatively low K_m value and a much higher k_{cat} value for NMN than the wild-type NadD (Table 1). The results were in good agreement with activity data from their corresponding RFP-fused counterparts (see above). The catalytic efficiency (k_{cat}/K_m) of the two mutants with respect to NMN was increased by 100-fold and 600-fold, respectively, compared to that of NadD (Table 1). However, these two mutants exhibited remarkably different kinetic traits for NaMN. That is, the 11B4 mutant had much lower catalytic efficiency for NaMN than NadD, while the 16D8 mutant had notably higher catalytic efficiency for NaMN. Therefore, the 11B4 mutant had completely shifted substrate specificity toward NMN, which should be valuable to enhance amidated NAD biosynthesis. The fact that the 16D8 mutant had improved catalytic efficiency for both NMN and NaMN suggested its potential to enhance both amidated and deamidated pathways.

TABLE 1 Kinetic parameters of wild-type NadD and its mutants

Enzyme	Kinetics for NMN			Kinetics for NaMN			Selectivity[a]	Fold change
	K_m (mM)	k_{cat} (s^{-1})	k_{cat}/K_m (mM^{-1} s^{-1})	K_m (mM)	k_{cat} (s^{-1})	k_{cat}/K_m (mM^{-1} s^{-1})		
NadD	9.4	0.76	0.08	0.11	4.9	44	1.8×10^{-3}	1
11B4	0.80	6.6	8.3	1.7	1.5	0.86	9.6	5,258
16D8	0.76	36	48	0.07	25	332	1.4×10^{-1}	78

[a](k_{cat}/K_m with NMN)/(k_{cat}/K_m with NaMN).

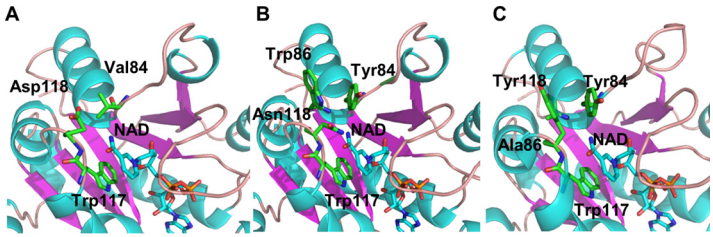

FIG 4 Homology models of complexes of the wild-type NaMNAT and mutants with NAD. (A) 11B4 (Y84V/Y118D). (B) 16D8 (A86W/Y118N). (C) Wild type of NadD. Structure modeling were generated using the Swiss-model server and the wild type of NadD (PDB ID: 1K4M) as the template. The protein structures are shown in cartoon mode, and the substrate and the residues are shown in stick mode.

Molecular modeling of NadD mutants. We performed molecular modeling in order to shed light on the mechanism of substrate recognition. The three-dimensional structures of mutants 11B4 and 16D8 were generated by the Swiss-model server using NadD (PDB identifier [ID]: 1K4M) as the template (Fig. 4). The 11B4 variant has Y84V and Y118D mutations (Fig. 4A), providing a negatively charged residue aspartic acid (pK_a of the β-carboxylate group, 3.65), which might incur a repulsion interaction with the carboxylate group (pK_a, 2.20) of the nicotinate and lead to decreased NaMN affinity. However, in terms of NMN, the side chain of the aspartic acid might form a hydrogen bond with the amide group of NMN, leading to increased NMN affinity, i.e., a lower K_m value of 0.80 mM. On the other hand, the side chain of V84 locates closer to the pyridine ring to form a more stable architecture, whereas Y84 in the wild-type protein has a phenolic group pointing toward the ligand but in the opposite direction. We presumed that V84 and D118 mutations play synergistic roles in substrate recognition and improved catalytic efficiency with respect to NMN.

In the wild-type enzyme, the main chain amide of A86 formed a water-bridged hydrogen bond to one oxygen atom of the nicotinate (Fig. 4C) (11). In the 16D8 mutant, A86 was replaced with tryptophan and Y118 replaced by asparagine (Fig. 4B). The indole ring of W86 and the aromatic ring of Y84 are almost parallel to each other and form a stable π-stacking interaction in the binding domain to stabilize the structure. The side chain of N118 has torsion due to the steric hindrance by W86 and points closer to the nicotinate or nicotinamide. Furthermore, the side chain of N118 can form an electronic interaction or hydrogen bonds with the exocylic carboxylate or carboxamido group of the mononucleotide. These molecular interactions may contribute enhanced affinity with both NMN and NaMN of 16D8 and result in better catalytic efficiency for both substrates.

Functional analysis of NadD mutants. To see if NadD mutants 11B4 and 16D8 can fully function *in vivo*, we cloned the mutant gene under the control of the *lac* promoter into *nadE* deletion strain *E. coli* YJE003. Because the last step of *de novo* NAD biosynthesis was blocked and endogenous amidated NAD biosynthesis was unable to produce enough NAD, YJE003 failed to grow even in nutrient-rich superoptimal broth (SOB) medium supplemented with NMN (9). Interestingly, NadD overexpression in YJE003 gave no apparent improvement in terms of cell viability (Fig. 5A). However, expression of the 16D8 mutant enabled cell growth on an SOB agar plate, while 11B4-expressing strain YJE003-11B4 required the presence of exogenous NMN or NAD. These results indicated that both mutants were functional in terms of catalyzing NAD formation *in vivo* via the amidated pathway. The reason that YJE003-11B4 failed to grow on an SOB agar plate might be attributable to the relatively low catalytic efficiency of 11B4. Indeed, the 11B4 mutant had a k_{cat} value for NMN that was about 5.5-fold lower than that of the 16D8 mutant. When supplemented with external NMN, YJE003-11B4 grew well, suggesting that a higher cellular NMN level was required for this less-efficient mutant to make enough NAD for cell survival. In order to clarify the function of 16D8 *in vivo*, we compared the cell growth profiles of the prototrophic BW25113 strain and YJE003-16D8 in M9 medium with glucose as the sole carbon source

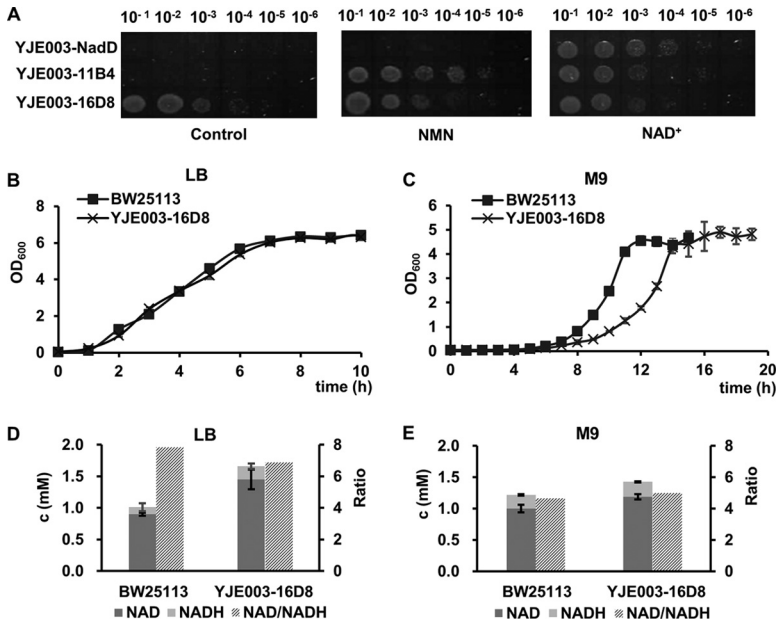

FIG 5 Growth profiles and NAD(H) levels of different *E. coli* strains. (A) Growth of YJE003-NadD, YJE003-11B4, and YJE003-16D8 on SOB agar plates. About 1×10^9 cells were suspended in 1 ml SOB agar, and 3 μl of aliquots at dilutions from 10^{-1} to 10^{-6} were spotted on SOB agar plates supplemented with appropriate antibiotics and IPTG. (B and C) Growth curves of *E. coli* BW25113 (■) and YJE003-16D8 (×) in LB (B) and M9 (C) medium at 37°C with an initial OD_{600} of 0.05. (D and E) Intracellular NAD(H) level and the ratio of NAD to NADH of BW25113 and YJE003-16D8 in LB (D) and M9 (E) medium in the stationary phase, respectively. Error bars represent the standard deviations of results from three independent cultures. c, concentration.

as well as with complex LB medium (Fig. 5B and C and Table 2). In LB medium, the lag phase of YJE003-16D8 was slightly longer than that of BW25113; however, there were no significant differences in terms of specific-growth rates. It was found that both BW25113 and YJE003-16D8 had a significantly longer lag phase (4.20 ± 0.08 h and 4.33 ± 0.04 h, respectively) in M9 medium and that YJE003-16D8 grew at a lower specific-growth rate (0.52 ± 0.01 h^{-1}) than the wild-type strain (0.78 ± 0.02 h^{-1}), suggesting that the amidated NAD pathway remained inferior to the native deaminated pathway in terms of supporting cell propagation. Interestingly, the biomass yield of YJE003-16D8 was higher than that of BW25113. In terms of the total NAD(H) level, YJE003-16D8 had 64% (*P* value, 0.007) more NAD(H) than the wild-type strain at the stationary phase in LB medium, while in M9 medium there was only slightly more NAD(H) found in YJE003-16D8 (Fig. 5D and E). Overall, these results indicated that the 16D8-mediated amidated pathway could function as the native deamidated pathway for cell survival under different environmental conditions.

DISCUSSION

In canonical *de novo* NAD biosynthesis, NaMN is adenylylated by NadD to form NaAD and is then amidated by NadE. In many bacteria, NadD also has residual activity

TABLE 2 Growth profile comparison between *E. coli* BW25113 and YJE003-16D8 cells[a]

	Value(s) for indicated strain in:					
	LB			M9		
Parameter	BW25113	YJE003-16D8	*P* value	BW25113	YJE003-16D8	*P* value
DCW (g/liter)	1.43 ± 0.02	1.42 ± 0.02	0.19	1.19 ± 0.00	1.65 ± 0.06	2.6×10^{-5}
Biomass yield (g/g)	NA	NA	NA	0.30 ± 0.00	0.41 ± 0.02	0.01
Lag phase (h)	0.18 ± 0.05	0.26 ± 0.03	0.02	4.20 ± 0.08	4.33 ± 0.04	0.03
Growth rate (h^{-1})	1.78 ± 0.29	1.67 ± 0.03	0.29	0.78 ± 0.02	0.52 ± 0.01	8.7×10^{-6}

[a]DCW, dry cell weight; NA, not available.

to adenylylate NMN for direct NAD synthesis. In *E. coli*, NadD strongly favors NaMN over NMN (9), but the molecular basis for such a substrate preference remains unclear. On the basis of structural data from the NadD-NaAD complex, we suggested that six amino acid residues might have major roles in substrate recognition. We constructed double-site saturation mutagenesis libraries and screened them by using a malic enzyme-coupled colorimetric assay. After two rounds of screening and further verification, two mutants, 11B4 (Y84V/Y118D) and 16D8 (A86S/Y118N), were identified with high activity with respect to synthesizing NAD with NMN and ATP. These results suggested that mutations at position 84, 86, and 118 had changed the substrate specificity and catalytic efficiency.

Our previous study showed that *E. coli* YJE003, which had its deamidated NAD biosynthetic pathway blocked due to *nadE* deletion, was unviable without NAD supplementation (10). The results suggested that NadD and NadR could not use intracellular NMN to produce enough NAD via the amidated pathway under physiological conditions (Fig. 1A), albeit both NadD and NadR showed inherent NMN adenylyltransferase activity *in vitro* (9, 19). Here, YJE003-NadD with multiple copies of the *nadD* gene remained unable to grow on a nutrient-rich SOB agar plate even with exogenous NMN supplementation, further confirming that the endogenous amidated pathway was insufficient for cellular NAD demands. Interestingly, expression of the 16D8 mutant in YJE003 facilitated cell growth in both complex medium and minimal medium, indicating that the significantly higher activity of NAD production was achieved via condensation of NMN and ATP, i.e., the amidated pathway. It is worth mentioning that YJE003-16D8 restored vitality to the same extent as prototrophic strain BW25113 in LB medium. Thus, the amidated pathway was engineered to full activity to maintain cell growth without a functional deamidated process.

It has been known that NAD homeostasis is tightly regulated by NadR via transcriptional repression of *nadA*, *nadB*, and *pncB* and by inhibiting NMN transportation when cellular NAD(H) is in excess (19). It has been demonstrated that overexpression of *pncB* under the control of a mutated promoter to prevent binding of the repressor NadR could lead to a 2-fold increase in the total NAD(H) level and to a 30%-higher NAD(H) level when *pncB* is under the control of the native promoter (3). Surprisingly, at the stationary phase of growth, *E. coli* YJE003-16D8 had a higher NAD(H) level than BW25113, suggesting that the engineered amidated NAD pathway was more effective than the native deamidated pathway for NAD biosynthesis. One possible reason is that the new pathway might escape from feedback inhibition.

The 16D8 mutant also enabled cell survival in the presence of external NMN, indicating that NMN played vital roles in cell survival. This is consistent with the phenomenon that YJE003-16D8 can synthesize NAD solely via the amidated pathway using NMN as the immediate precursor for survival. These observations are puzzling as our current knowledge suggests that NAD homeostasis cannot be maintained by *de novo* NMN formation in *E. coli* (Fig. 1A). While *de novo* formation of NaMN and NA remains active in YJE003-16D8, no enzymes capable of converting NaMN to NMN, or NA to Nm, have been characterized previously. It is known that PncC-catalyzed deamination of NMN is irreversible (19, 20) in *E. coli*, but whether PncA could catalyze the reversible reaction, namely, amidation of NA to Nm (21), is unclear. Nonetheless, we assume that amidation of either NaMM or NA by an elusive enzyme(s) occurs in YJE003-16D8 and leads to fueling of the amidated pathway with precursors from *de novo* NAD biosynthesis. It will be interesting to look into this issue in a future study.

In summary, we devised *E. coli* NadD mutants to use NMN as the favored substrate and achieved a fully active amidated pathway for NAD biosynthesis. The information is valuable for manipulation of cellular NAD metabolism and for further exploration of the substrate specificity of other examples of NMNAT for synthesis of cofactor analogs.

MATERIALS AND METHODS

General procedures. FastPfu DNA polymerase was purchased from Transgen (Shanghai, China). PrimeSTAR HS DNA polymerase and DpnI were purchased from TaKaRa (Dalian, China). NMN, NaMN,

TABLE 3 Strains and plasmids used in this study

Strain or plasmid	Genotype or characteristic	Source or reference
E. coli strains		
DH10b	F$^-$ *endA1 deoR recA1 galE15 galK16 nupG rpsL*Δ(*lac*)*X74* ϕ80*lacZ*ΔM15 *araD139* Δ(*ara leu*)*7697 mcrA* Δ(*mrr-hsdRMS-mcrBC*) Str^r[a] λ^-	Invitrogen
BL21(DE3)	F$^-$ *dcm ompT hsdS*(r_B^-, m_B^-) λ(DE3)	Novagen
BW25113	*rrnB3* Δ*lacZ4787 hsdR514* Δ(*araBAD*)*567* Δ(*rhaBAD*)*568 rph-1*	CGSC
YJE003	BW25113/pET-15K-NTT4/*nadE*::*cat*	10
YJE003-NadD	YJE003, pA-NadD	This study
YJE003-11B4	YJE003, pA-NadD-11B4	This study
YJE003-16D8	YJE003, pA-NadD-16D8	This study
Plasmids		
pUC18	*lacZ*, *pBR322 ori*, *bla*, cloning vector	TaKaRa
pUC-RFP	pUC18 with *lacZ* replaced by *rfp* gene, *bla*::*kan*	This study
pUR-NadD	pK with *lacZ* replaced by *nadD-rfp* fusion gene	This study
pUC-NadE	pK with *lacZ* replaced by *nadE* gene	This study
pUC-NadD	pK with *lacZ* replaced by *nadD* gene	This study
pA-NadD	pUC18 with *lacZ* replaced by *nadD* gene	This study
pA-NadD-11B4	pUC18 with *lacZ* replaced by *nadD*-11B4 gene	This study
pA-NadD-16D8	pUC18 with *lacZ* replaced by *nadD*-16D8 gene	This study

[a]Str^r, streptomycin resistance.

alcohol dehydrogenase (ADH II), phenazine methosulfate (PMS), nitroblue tetrazolium (NBT), phenazine ethosulfate (PES), methylthiazolyldiphenyl-tetrazolium bromide (MTT), and isopropyl-β-thiogalactoside (IPTG) were purchased from Sigma-Aldrich (St. Louis, MO, USA). ATP, kanamycin, and lysozyme were purchased from Sangon Biotech (Shanghai, China). The strains and plasmids that we used are listed in Table 3. Primers (Table 4) were synthesized by Sangon Biotech (Shanghai, China). Red fluorescent protein (RFP) gene (22) *rfp* was synthesized by Synbio-tech (Suzhou, China).

Plasmid construction. A restriction-free cloning method (23) was used for plasmid construction.

The original pUC-RFP plasmid was constructed by simultaneously replacing the ampicillin resistance gene and α-peptide gene with the kanamycin resistance gene from pKD4 and *rfp* in pUC18, respectively. The kanamycin resistance gene was amplified by primers pUC-RFP-s and pUC-RFP-a, while the *rfp* gene was amplified by Kan-F and Kan-R.

The NadD-RFP fusion expression plasmid was constructed by inserting the *nadD* gene and the DNA fragment GGAGGAGGATCA coding for a GGGS linker between the *lac* promoter and the *rfp* gene in pUC-RFP vector. Briefly, the *nadD* gene was amplified from the genomic DNA of BL21(DE3) by using primers pUR-nadD-s and pUR-nadD-a. The gel-purified products were used as megaprimer, and plasmid pUC-RFP was used as the template for linear amplification. After DpnI digestion, the PCR products were transformed into electroporation-competent DH10b cells. The translation product of the resulting

TABLE 4 Oligonucleotide primers used in this study

Primer name	Primer sequence (5′→3′)[a]
pUC-RFP-s	ggataacaatttcacacaggaaacaCATATGGCTTCCTCCGAAGACGTTATC
pUC-RFP-a	gtgtcggggctggcttaatcaGTGGTGGTGGTGGTGGTGAGCACCGGTGGAGTGAC GACCTTC
Kan-F	aatacattcaaatatgtatccgctcatgAGAATAGGAACTTCGGAATAGG
Kan-R	agattatcaaaaaggatcttcaccTAGATCGAACTTCAGAGCGCTTTTG
pUR-nadD-s	ggataacaatttcacacaggaaacaCATATGAAATCTTTACAGGCTCTGTTTGG
pUR-nadD-a	ctttgataacgtcttcggaggaagccatTGATCCTCCTCCGCGATACAAGCCTTGTTGG
pUC-nadE-s	ggataacaatttcacacaggaaacaCATATGACATTGCAACAACAAATAATAAAGG
pUC-nadE-a	gctggcttaatcagtggtggtggtggtggtgCTTTTTCCAGAAATCATCGAAAACG
NadD-H45X-s	ggtcacaatcatccctaataatgttcctccgNNKcgtccccagccggaagcgaacagc
NadD-Y84X-s	gctaaagcgcaatgccccctctNNKactgcgcaaacactgaaagagtgg
NadD-T85X-s	gctaaagcgcaatgccccctcttacNNKgcgcaaacactgaaagagtgg
NadD-A86X-s	gctaaagcgcaatgccccctcttacactNNKcaaacactgaaagagtggcggcagg
NadD-T85XA86X-s	gctaaagcgcaatgccccctcttacNNKNNKcaaacactgaaagagtgg
NadD-P82X-a	ccactctttcagtgtttgcgcagtgtaagaMNNggcattgcgctttagctcg
NadD-T85X-a	ccactctttcagtgtttgcgcMNNgtaagaggggggcattgcgctttagctcg
NadD-Y118X-a	gcattgtcgagtatcgtttcgtattcMNNccaggtcggaaaggtcagcagtgaatcc
NadD-P82XY84X-s	cgagctaaagcgcaatgccNNKtctNNKactgcgcaaacactgaaagagtgg
RFP-deletion-a	gcttaatcagtggtggtggtggtggtgGCGATACAAGCCTTGTTGG
pUC-D	cgtttcggtgatgacggtg

[a]Underlining indicates the target sites for mutation; lowercase indicates homology regions.

plasmid would be a fusion protein (NadD-RFP) with a GGGS linker between the two domains and a His_6 tag in the C terminus.

The NAD synthetase NadE expression plasmid was constructed by replacing *nadE* with *rfp* in plasmid pUC-RFP. Briefly, the *nadE* gene was amplified from BL21(DE3) genomic DNA by the use of primers pUC-nadE-s and pUC-nadE-a. The gel-purified products were inserted into pUC-RFP. The PCR products present after DpnI digestion were transformed into DH10b. The resulting expression vector was termed pUC-NadE.

The NadD and mutant expression plasmids without RFP were constructed by deleting the *rfp* open reading frame in their corresponding RFP fusion plasmids. Briefly, primer pair pUR-NadD-s/RFP-deletion-a was used to amplify *nadD* and the mutant gene without the *rfp* gene. The purified fragments were then used as a megaprimer, and their parental plasmids were used as the templates. The PCR products were digested with DpnI and transformed into DH10b. The resulting plasmids could produce NadD and mutant protein with a 6-histidine tag at the carboxy terminus.

For complementation experiments, the NadD and mutant expression plasmids were constructed by inserting *nadD* and the mutant gene into pUC18. Briefly, primer pair pUR-NadD-s/pUC-D was used to amplify the *nadD*, *nadD*-11B4, and *nadD*-16D8 genes and then the purified fragments were subcloned into pUC18. The PCR products were digested with DpnI and transformed into DH10b. The correct vectors harboring ampicillin resistance were designated pA-NadD, pA-NadD-11B4, and pA-NadD-16D8.

Site saturation mutagenesis. Double-site saturation mutant libraries were constructed by the use of degenerated primers as described previously (24). The target amino acids were coded by NNK (forward; N, adenine/cytosine/guanine/thymine; K, guanine/thymine) and MNN (reverse; M, adenine/cytosine). The pUR-NadD plasmid was used as the template. Target residues and the degenerate primers are listed in Table 1. The mutant fragments were cloned into pUR-NadD. The PCR products were treated with DpnI to digest the methylated parental plasmid and were transformed into the electrocompetent DH10b cells.

Library screening. A total of 2,000 individual colonies from each library were picked up and inoculated in 200 μl LB medium containing tryptone (10 g/liter), yeast extract (5 g/liter), NaCl (10 g/liter), kanamycin (50 μg/ml), and 0.2 mM IPTG in 96-well deep plates. The cultures were grown at 30°C and 200 rpm for 72 h. Cells were harvested by centrifugation at 2,100 $\times$ *g* for 15 min. The pellets were resuspended and lysed with 50 μl lysis buffer containing 50 mM HEPES (pH 7.5), 1% (vol/vol) Triton X-100, and lysozyme (1 mg/ml) at 37°C for 2 h. The supernatant containing soluble crude enzyme was collected by centrifugation as described above.

A colorimetric high-throughput assay was employed for the initial screening of the mutant libraries. Briefly, a volume of 50 μl of a substrate mixture containing 5 mM $MnCl_2$, 10 mM $MgCl_2$, 2 mM ATP, 10 μl crude enzyme, and 50 mM HEPES (pH 7.5) was shaken at 37°C and 200 rpm for 2 h. Then, a volume of 10 μl of a dye mixture containing 5 mM $MnCl_2$, 10 mM $MgCl_2$, 30 mM L-malate, 0.15 mM PMS, 0.6 mM NBT, 50 mM HEPES (pH 7.5), and 0.06 U purified malic enzyme (25) was added and incubated at room temperature for 1 h. The accumulation of formazan crystals, which are formed by the reduction of NBT (26), was visually examined.

Confirmatory screening was carried out to further confirm the activity of the suspected mutants. The colonies were grown in a volume of 2.5 ml LB medium supplemented with kanamycin (50 μg/ml) and 0.2 mM IPTG in 24-well deep plates. The plates were shaken at 30°C for 48 h. The cell pellets present after centrifugation were resuspended with 300 μl lysis buffer, and 100 μl supernatant was incubated with 300 μl of the substrate mixture at 37°C and 200 rpm for 2 h. The detection method was the same as that used for the initial screening.

Crude enzyme activities were measured by an endpoint assay. The strains were cultured and induced in 5 ml LB, and the cell pellets were treated with 500 μl cell lysis buffer. We added 100 μl of crude enzyme into 300 μl of a substrate mixture containing 100 μM NMN and 2 mM ATP, and the mixture was maintained for 2 h at 37°C. The reaction was quenched by adding an equal volume of chloroform. After centrifugation at 14,200 $\times$ *g* for 15 min, we transferred 45 μl of supernatant into 100 μl of dye mixture containing 5 mM $MnCl_2$, 10 mM $MgCl_2$, 5 mM L-malate, 0.4 mM PES, 1 mM MTT, 0.8 U purified malic enzyme, and 50 mM HEPES (pH 7.5). The absorbance at 570 nm was monitored at room temperature with a PowerWave XS universal microplate spectrophotometer (Bio-Tek Instruments Inc., USA).

To validate the mutant sites, plasmids from the positive hits were extracted and sequenced by Sangon Biotech (Shanghai, China).

Protein expression and purification. Cells were grown in LB medium containing kanamycin (50 μg/ml) at 37°C until an optical density at 600 nm (OD_{600}) of 0.6 was reached. The culture was then supplemented with 0.2 mM IPTG and incubated at 30°C for 16 h. Cells were collected by centrifugation at 11,300 $\times$ *g* for 10 min and resuspended in Native binding buffer (50 mM NaH_2PO_4, 0.5 M NaCl, 10 mM imidazole, pH 8.0) and sonicated. The supernatant present after centrifugation at 21,800 $\times$ *g* for 30 min was loaded onto a nickel-nitrilotriacetic acid (Ni-NTA) column. The column was washed with Native washing buffer (50 mM NaH_2PO_4, 0.5 M NaCl, 40 mM imidazole, pH 8.0), and the target protein was then eluted with Native elution buffer (50 mM NaH_2PO_4, 0.5 M NaCl, 250 mM imidazole, pH 8.0). Imidazole was removed, and the buffer was replaced with protein storage buffer containing 50 mM Tris (pH 7.5), 50 mM NaCl, and 5% (vol/vol) glycerol. The concentration of the purified protein was determined using the Bradford method (27) with bovine serum albumin as the standard.

Enzyme activity assay. Purified-enzyme activity was evaluated by a continuous optical method. Standard reaction mixtures (100 μl) contained 5 mM $MnCl_2$, 10 mM $MgCl_2$, 100 μM NMN, 2 mM ATP, 10 mM L-malate, 0.4 mM PES, 1 mM MTT, 1 U purified malic enzyme, 0.1 to 0.5 mg mutant enzyme, and 50 mM HEPES (pH 7.5). The absorbance at 570 nm was monitored as described above.

Kinetic characterization. Levels of NaMN and NMN adenylyltransferase activity were measured by coupling performed with alcohol dehydrogenase, reducing NAD to NADH as described previously (28) with slight modifications. A reduced volume of 150 μl assay mixture contained 4 mM ATP, 10 mM $MgCl_2$, 45.8 mM ethanol, 7.06 U/ml alcohol dehydrogenase, approximately 100 to 8,000 μM NMN, and 100 mM Tris (pH 8.0). To evaluate the NaMN-specific activity, the reaction mixture was also supplemented with 10 mM NH_4Cl and an excess of NadE from BL21(DE3). The reaction was started by adding purified enzyme at levels of from 0.3 to 3 μg and was monitored by the change in UV absorbance at 340 nm using a spectrophotometer at 25°C. The kinetic data were determined from a Lineweaver-Burk plot.

Structural modeling. The three-dimensional structures of NadD mutants 11B4 and 16D8 were generated computationally by the Swiss model server (29) (https://swissmodel.expasy.org/). The crystal structure of wild-type NadD (PDB ID: 1K4M) was used as the template.

***In vivo* functional evaluation.** *E. coli* YJE003 electrocompetent cells were transformed separately using plasmid pUC18, plasmid pA-NadD-WT, plasmid pA-NadD-11B4, or plasmid pA-NadD-16D8. The transformants were cultured in SOB medium containing tryptone (2 g/liter), yeast extract (0.5 g/liter), NaCl (0.05 g/liter), 2.5 mM KCl, 10 mM $MgCl_2$, kanamycin (50 μg/ml), ampicillin (100 μg/ml), chloromycetin (34 μg/ml), 0.1 mM IPTG, and 0.5 mM NAD at 37°C and 200 rpm for 14 h. About 1×10^9 cells were collected and washed thrice using 1 ml of SOB medium and then resuspended in 1 ml of SOB medium. A 3-μl volume of dilutions from 10^{-1} to 10^{-6} was spotted on the corresponding SOB agar plates containing kanamycin (50 μg/ml), chloromycetin (34 μg/ml), ampicillin (100 μg/ml), and 0.1 mM IPTG. The plates were cultured at 37°C for 14 h.

To determine the growth curve of the strains, the cells were cultured overnight and then collected and washed thrice with 1 ml of synthetic M9 medium containing glucose (4 g/liter), NaCl (0.5 g/liter), NH_4Cl (1 g/liter), 42 mM Na_2HPO_4, 22 mM KH_2PO_4, 2 mM $MgSO_4$, and 0.1 mM $CaCl_2$ and were then inoculated into 50 ml of M9 medium with an initial OD_{600} of 0.025 and cultivated at 37°C and 200 rpm. The absorbance at 600 nm was measured every 2 h. The specific-growth rate and lag-phase data were estimated from absorbance growth curves using the modified Gompertz model as described previously (30). The *P* values were calculated by the independent-sample *t* test.

Intracellular NAD(H) was extracted, and levels were determined by using alcohol dehydrogenase-linked assays as described previously (31).

SUPPLEMENTAL MATERIAL

Supplemental material for this article may be found at https://doi.org/10.1128/AEM.00692-17.

SUPPLEMENTAL FILE 1, PDF file, 0.2 MB.

ACKNOWLEDGMENTS

We thank Debin Ji, Yixin Zhang, and Hongdi Liu for helpful suggestions and comments on the manuscript. We also thank Xinping Lin, Xiaojia Guo, and Xiaobing Yang for helpful suggestions and discussion regarding this project.

This work was supported by National Natural Science Foundation of China (no. 21325627 and 51561145014).

REFERENCES

1. Zhang X, Wang X, Shanmugam KT, Ingram LO. 2011. L-Malate production by metabolically engineered *Escherichia coli*. Appl Environ Microbiol 77:427–434. https://doi.org/10.1128/AEM.01971-10.
2. Zhou YJ, Yang W, Wang L, Zhu Z, Zhang S, Zhao ZK. 2013. Engineering NAD^+ availability for *Escherichia coli* whole-cell biocatalysis: a case study for dihydroxyacetone production. Microb Cell Fact 12:103. https://doi.org/10.1186/1475-2859-12-103.
3. San KY, Bennett GN, Berrios-Rivera SJ, Vadali RV, Yang YT, Horton E, Rudolph FB, Sariyar B, Blackwood K. 2002. Metabolic engineering through cofactor manipulation and its effects on metabolic flux redistribution in *Escherichia coli*. Metab Eng 4:182–192. https://doi.org/10.1006/mben.2001.0220.
4. Steen EJ, Kang YS, Bokinsky G, Hu ZH, Schirmer A, McClure A, del Cardayre SB, Keasling JD. 2010. Microbial production of fatty-acid-derived fuels and chemicals from plant biomass. Nature 463:559–562. https://doi.org/10.1038/nature08721.
5. Chang MCY, Eachus RA, Trieu W, Ro DK, Keasling JD. 2007. Engineering *Escherichia coli* for production of functionalized terpenoids using plant P450s. Nat Chem Biol 3:274–277. https://doi.org/10.1038/nchembio875.
6. Gerdes SY, Scholle MD, D'Souza M, Bernal A, Baev MV, Farrell M, Kurnasov OV, Daugherty MD, Mseeh F, Polanuyer BM, Campbell JW, Anantha S, Shatalin KY, Chowdhury SAK, Fonstein MY, Osterman AL. 2002. From genetic footprinting to antimicrobial drug targets: examples in cofactor biosynthetic pathways. J Bacteriol 184:4555–4572. https://doi.org/10.1128/JB.184.16.4555-4572.2002.
7. D'Angelo I, Raffaelli N, Dabusti V, Lorenzi T, Magni G, Rizzi M. 2000. Structure of nicotinamide mononucleotide adenylyltransferase: a key enzyme in NAD^+ biosynthesis. Structure 8:993–1004. https://doi.org/10.1016/S0969-2126(00)00190-8.
8. Magni G, Di Stefano M, Orsomando G, Raffaelli N, Ruggieri S. 2009. NAD(P) biosynthesis enzymes as potential targets for selective drug design. Curr Med Chem 16:1372–1390. https://doi.org/10.2174/092986709787846505.
9. Mehl RA, Kinsland C, Begley TP. 2000. Identification of the *Escherichia coli* nicotinic acid mononucleotide adenylyltransferase gene. J Bacteriol 182:4372–4374. https://doi.org/10.1128/JB.182.15.4372-4374.2000.
10. Zhou Y, Wang L, Yang F, Lin X, Zhang S, Zhao ZK. 2011. Determining the extremes of the cellular NAD(H) level by using an *Escherichia coli* NAD^+-auxotrophic mutant. Appl Environ Microbiol 77:6133–6140. https://doi.org/10.1128/AEM.00630-11.
11. Zhang H, Zhou T, Kurnasov O, Cheek S, Grishin NV, Osterman A. 2002. Crystal structures of *E. coli* nicotinate mononucleotide adenylyltransferase and its complex with deamido-NAD. Structure 10:69–79. https://doi.org/10.1016/S0969-2126(01)00693-1.
12. Stancek M, Schnell R, Ryden-Aulin M. 2005. Analysis of *Escherichia coli* nicotinate mononucleotide adenylyltransferase mutants *in vivo* and *in vitro*. BMC Biochem 6:16. https://doi.org/10.1186/1471-2091-6-16.

13. Stancek M, Isaksson LA, Ryden-Aulin M. 2003. *fusB* is an allele of *nadD*, encoding nicotinate mononucleotide adenylyltransferase in *Escherichia coli*. Microbiology 149:2427–2433. https://doi.org/10.1099/mic.0.26337-0.
14. Sun Z, Lonsdale R, Wu L, Li G, Li A, Wang J, Zhou J, Reetz MT. 2016. Structure-guided triple-code saturation mutagenesis: efficient tuning of the stereoselectivity of an epoxide hydrolase. ACS Catal 6:1590–1597. https://doi.org/10.1021/acscatal.5b02751.
15. Duine JA. 1991. Cofactor engineering. Trends Biotechnol 9:343–346. https://doi.org/10.1016/0167-7799(91)90116-Y.
16. Zhai RG, Rizzi M, Garavaglia S. 2009. Nicotinamide/nicotinic acid mononucleotide adenylyltransferase, new insights into an ancient enzyme. Cell Mol Life Sci 66:2805–2818. https://doi.org/10.1007/s00018-009-0047-x.
17. Lau C, Niere M, Ziegler M. 2009. The NMN/NaMN adenylyltransferase (NMNAT) protein family. Front Biosci 14:410–431. https://doi.org/10.2741/3252.
18. Waldo GS, Standish BM, Berendzen J, Terwilliger TC. 1999. Rapid protein-folding assay using green fluorescent protein. Nat Biotechnol 17:691–695. https://doi.org/10.1038/10904.
19. Raffaelli N, Lorenzi T, Mariani PL, Emanuelli M, Amici A, Ruggieri S, Magni G. 1999. The *Escherichia coli* NadR regulator is endowed with nicotinamide mononucleotide adenylyltransferase activity. J Bacteriol 181:5509–5511.
20. Sorci L, Martynowski D, Rodionov DA, Eyobo Y, Zogaj X, Klose KE, Nikolaev EV, Magni G, Zhang H, Osterman AL. 2009. Nicotinamide mononucleotide synthetase is the key enzyme for an alternative route of NAD biosynthesis in *Francisella tularensis*. Proc Natl Acad Sci U S A 106:3083–3088. https://doi.org/10.1073/pnas.0811718106.
21. Frothingham R, Meeker-O'Connell WA, Talbot EAS, George JW, Kreuzer KN. 1996. Identification, cloning, and expression of the *Escherichia coli* pyrazinamidase and nicotinamidase gene, *pncA*. Antimicrob Agents Chemother 40:1426–1431.
22. Campbell RE, Tour O, Palmer AE, Steinbach PA, Baird GS, Zacharias DA, Tsien RY. 2002. A monomeric red fluorescent protein. Proc Natl Acad Sci U S A 99:7877–7882. https://doi.org/10.1073/pnas.082243699.
23. Unger T, Jacobovitch Y, Dantes A, Bernheim R, Peleg Y. 2010. Applications of the restriction free (RF) cloning procedure for molecular manipulations and protein expression. J Struct Biol 172:34–44. https://doi.org/10.1016/j.jsb.2010.06.016.
24. van den Ent F, Lowe J. 2006. RF cloning: a restriction-free method for inserting target genes into plasmids. J Biochem Biophys Methods 67:67–74. https://doi.org/10.1016/j.jbbm.2005.12.008.
25. Wang J, Tan H, Zhao ZK. 2007. Over-expression, purification, and characterization of recombinant NAD-malic enzyme from *Escherichia coli* K12. Protein Expr Purif 53:97–103. https://doi.org/10.1016/j.pep.2006.11.017.
26. Mayer KM, Arnold FH. 2002. A colorimetric assay to quantify dehydrogenase activity in crude cell lysates. J Biomol Screen 7:135–140. https://doi.org/10.1177/108705710200700206.
27. Bradford MM. 1976. A rapid and sensitive method for the quantitation of microgram quantities of potein utilizing the principle of protein-dye binding. Anal Biochem 72:248–154. https://doi.org/10.1016/0003-2697(76)90527-3.
28. Balducci E, Emanuelli M, Raffaelli N, Ruggieri S, Amici A, Magni G, Orsomando G, Polzonetti V, Natalini P. 1995. Assay methods for nicotinamide mononucleotide adenylyltransferase of wide applicability. Anal Biochem 228:64–68. https://doi.org/10.1006/abio.1995.1315.
29. Lauck F, Smith CA, Friedland GF, Humphris EL, Kortemme T. 2010. RosettaBackrub—a web server for flexible backbone protein structure modeling and design. Nucleic Acids Res 38:569–575. https://doi.org/10.1093/nar/gkq369.
30. Zwietering MH, Jongenburger I, Rombouts FM, Riet KV. 1990. Modeling of the bacterial growth curve. Appl Environ Microbiol 56:1875–1881.
31. Kern SE, Price-Whelan A, Newman DK. 2014. Extraction and measurement of NAD(P)$^+$ and NAD(P)H. Methods Mol Biol 1149:311–323. https://doi.org/10.1007/978-1-4939-0473-0_26.